Prediction of Individual Disease Conversion in Early AMD Using Artificial Intelligence

Ursula Schmidt-Erfurth,[1] Sebastian M. Waldstein,[1] Sophie Klimscha,[1] Amir Sadeghipour,[1] Xiaofeng Hu,[1] Bianca S. Gerendas,[1] Aaron Osborne,[2] and Hrvoje Bogunović[1]

[1]Christian Doppler Laboratory for Ophthalmic Image Analysis, Vienna Reading Center, Department of Ophthalmology, Medical University of Vienna, Vienna, Austria
[2]Genentech, Inc., South San Francisco, California, United States

Correspondence: Ursula Schmidt-Erfurth, Department of Ophthalmology, Medical University of Vienna, Spitalgasse 23, 1090 Vienna, Austria; ursula.schmidt-erfurth@meduniwien.ac.at.

Submitted: February 14, 2018
Accepted: June 1, 2018

Citation: Schmidt-Erfurth U, Waldstein SM, Klimscha S, et al. Prediction of individual disease conversion in early AMD using artificial intelligence. *Invest Ophthalmol Vis Sci*. 2018;59:3199–3208. https://doi.org/10.1167/iovs.18-24106

Purpose. While millions of individuals show early age-related macular degeneration (AMD) signs, yet have excellent vision, the risk of progression to advanced AMD with legal blindness is highly variable. We suggest means of artificial intelligence to individually predict AMD progression.

Methods. In eyes with intermediate AMD, progression to the neovascular type with choroidal neovascularization (CNV) or the dry type with geographic atrophy (GA) was diagnosed based on standardized monthly optical coherence tomography (OCT) images by independent graders. We obtained automated volumetric segmentation of outer neurosensory layers and retinal pigment epithelium, drusen, and hyperreflective foci by spectral domain-OCT image analysis. Using imaging, demographic, and genetic input features, we developed and validated a machine learning–based predictive model assessing the risk of conversion to advanced AMD.

Results. Of a total of 495 eyes, 159 eyes (32%) had converted to advanced AMD within 2 years, 114 eyes progressed to CNV, and 45 to GA. Our predictive model differentiated converting versus nonconverting eyes with a performance of 0.68 and 0.80 for CNV and GA, respectively. The most critical quantitative features for progression were outer retinal thickness, hyperreflective foci, and drusen area. The features for conversion showed pathognomonic patterns that were distinctly different for the neovascular and the atrophic pathways. Predictive hallmarks for CNV were mostly drusen-centric, while GA markers were associated with neurosensory retina and age.

Conclusions. Artificial intelligence with automated analysis of imaging biomarkers allows personalized prediction of AMD progression. Moreover, pathways of progression may be specific in respect to the neovascular/atrophic type.

Keywords: age-related macular degeneration, optical coherence tomography, machine learning, artificial intelligence, choroidal neovascularization

Age-related macular degeneration (AMD) is a leading cause for irreversible visual loss despite progress in therapeutic strategies. As a result of shifting demographics and aging populations, rates of overall worldwide vision loss during 2005–2015 increased by 23% for blindness and by 24% for severe vision impairment, in total affecting more than 900 million individuals.[1] Impaired visual function has a tangible impact on quality of life, with sight loss being independently associated with adverse social outcomes and impaired general and mental health.[2] There is obviously an urgent need to intervene in a timely manner, to efficiently manage the consequences of this overwhelming epidemic, and to understand the association of ageing and invariable vision loss.

Progression to advanced AMD is heralded by the presence of large drusen and pigmentary anomalies.[3] However, despite these associations on a population level, it is difficult to determine the precise risk and timing of disease progression for an individual patient.

With rapid advances in diagnostic imaging technology, the morphologic assessment of macular pathology has shifted to optical coherence tomography (OCT).[4] Spectral domain (SD)-OCT was successful in reliably detecting drusen in 99.7% of AMD eyes in the Age-Related Eye Disease Study (AREDS) cohort.[5] Quantitative drusen imaging revealed a dynamic growth pattern of drusen with an increase in drusen volume over time in 48% of eyes.[6] Moreover, a distinct association was found between drusen characteristics such as area and volume and the development of advanced AMD, both for the neovascular as well as atrophic type.[7] Since patients with a high drusen volume have a significantly higher progression rate toward either form of advanced AMD, OCT algorithms capable of reliably measuring drusen were suggested for determining clinical trial endpoints for AMD, accelerating the development of timely and adequate treatments.[8]

Advanced means of medical image analysis are now beginning to offer tools that are not only able to automatically and reliably segment even discrete morphologic features and to recognize associations between markers, identifying pathophysiological patterns, but also to offer distinct predictions of the future disease course.[9]

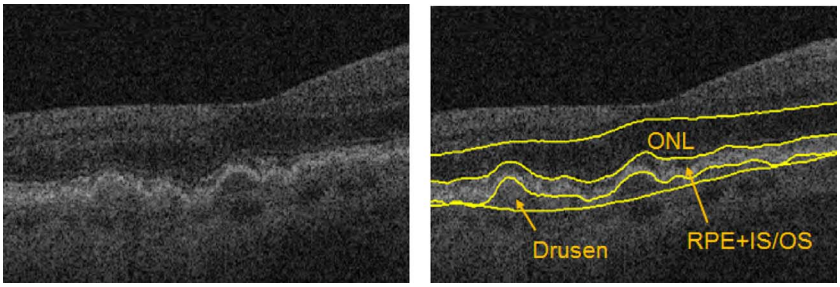

Figure 1. Example of automated outer retinal layer segmentation (overlaid in *yellow*): ONL, RPE, and IS/OS, as well as drusen/pseudodrusen.

In this article, we present a method to identify the individual risk of conversion of intermediate AMD to the advanced stages, that is, neovascular AMD or geographic atrophy (GA). We describe how modern means of artificial intelligence such as machine learning techniques can be used to predict the individual risk of disease progression in a common and severe disease such as AMD based mainly on morphologic imaging biomarkers but also on integrating genetic and demographic parameters.

Methods

Participants and Image Acquisition

This post hoc analysis was performed on longitudinal data of fellow eyes of patients with neovascular AMD participating in the HARBOR clinical trial (ClinicalTrials.gov identifier: NCT00891735). HARBOR was a 24-month, phase III, randomized, multicenter, double-masked, active treatment controlled study that evaluated the efficacy and safety of intravitreal ranibizumab, 0.5 and 2.0 mg, administered monthly or on an as-needed basis in 1095 treatment-naive patients with subfoveal neovascular AMD. Patients had prospective monthly evaluations of both eyes with SD-OCT imaging following a standardized protocol. All images in the study were acquired with a HD-OCT device (Cirrus; Carl Zeiss Meditec, Inc., Dublin, CA, USA) and contained $512 \times 128 \times 1024$ voxels with a size of $11.7 \times 47.2 \times 2.0$ μm^3, covering a volume of $6 \times 6 \times 2$ mm^3. The study was conducted in compliance with the Declaration of Helsinki, and approval for this post hoc analysis was obtained by the Ethics Committee at the Medical University of Vienna.

Manual Grading Protocol

To create a gold standard of conversion times, two graders (SK, XH) manually determined the time of first conversion to advanced AMD, characterized by either choroidal neovascularization (CNV) or GA, for each fellow eye on the basis of OCT imaging. As previously defined by Abdelfattah et al.,[8] presence of intraretinal fluid (IRC) or subretinal fluid (SRF) with an associated suspicious pigment epithelial detachment (PED) or subretinal hyperreflective material (SHRM) was considered as evidence of CNV. Furthermore, the presence of thinning of the RPE band, loss of the overlying ellipsoid zone (EZ), and external limiting membrane (ELM) with thinning of the outer nuclear layer (ONL) as well as an increased signal transmission into the choroid were regarded as GA.

Automated Image Analysis

To be able to quantitatively characterize the morphology of the retina, a series of fully automated image analysis steps without manual correction was performed with the aim of extracting and measuring OCT biomarkers associated with AMD. The specific biomarkers of interest were the status of outer retinal layers, drusen and reticular pseudodrusen, and hyperreflective foci (HRF).

Retinal Layer Segmentation. Automated layer segmentation was based on the Iowa Reference Algorithms,[10] a graph theoretic approach for identifying a set of surfaces corresponding to layer interfaces. The following three layers denoting the outer retina were segmented and their thickness measured: ONL, RPE with photoreceptor outer segments (RPE+IS/OS), and drusen space between the RPE and Bruch's membrane. An example of the segmentation of the three retinal layers is shown in Figure 1.

Drusen and Reticular Pseudodrusen Segmentation. The thickness of the segmented drusen was thresholded to obtain an en face retinal region covered by drusen, which we call the drusen footprint (see Fig. 4). In addition, automated image segmentation based on watershed transform was applied to further partition drusen into individual ones. The reticular pseudodrusen were segmented by thresholding bright voxels overlying the IS/OS layer, identifying reflective objects that protruded into the interface between the IS/OS and ONL layers.

HRF Segmentation. HRF were automatically segmented with a deep learning approach based on a convolutional neural network (CNN)[11] specifically developed for this purpose. The CNN was trained on 812 manually annotated B-scans containing HRF from 104 patients with CNV, diabetic macular edema, or retinal vein occlusion. The training set scans were acquired with two different OCT device models (Cirrus; Carl Zeiss, and Spectralis; Heidelberg Engineering, Heidelberg, Germany) and were separate from the set of scans used in our study. Representative HRF segmentations are shown in Figure 2.

Predictive Modeling

Machine learning builds predictive models by learning from examples. Here we learn the risk of conversion from a set of automatically computed eye characteristics and their manually graded conversion intervals. Each eye was characterized with a set of quantitative imaging and nonimaging features. Image-based features characterized the morphology of the retina while demographic and genetic features characterized the patient. To characterize the change of retinal morphology across time, in addition to the baseline scan, we took the four next monthly follow-up scans into consideration. A predictive model was then created that learned from the features of the 4-month observation period to predict the risk of conversion in the remaining period of the 2-year study (Fig. 3).

Image-Based Features. From the image analysis steps, imaging biomarkers of interest were represented as two-dimensional (2D) en face thickness maps from which a large and diverse set of features was computed as listed in Table 1. In

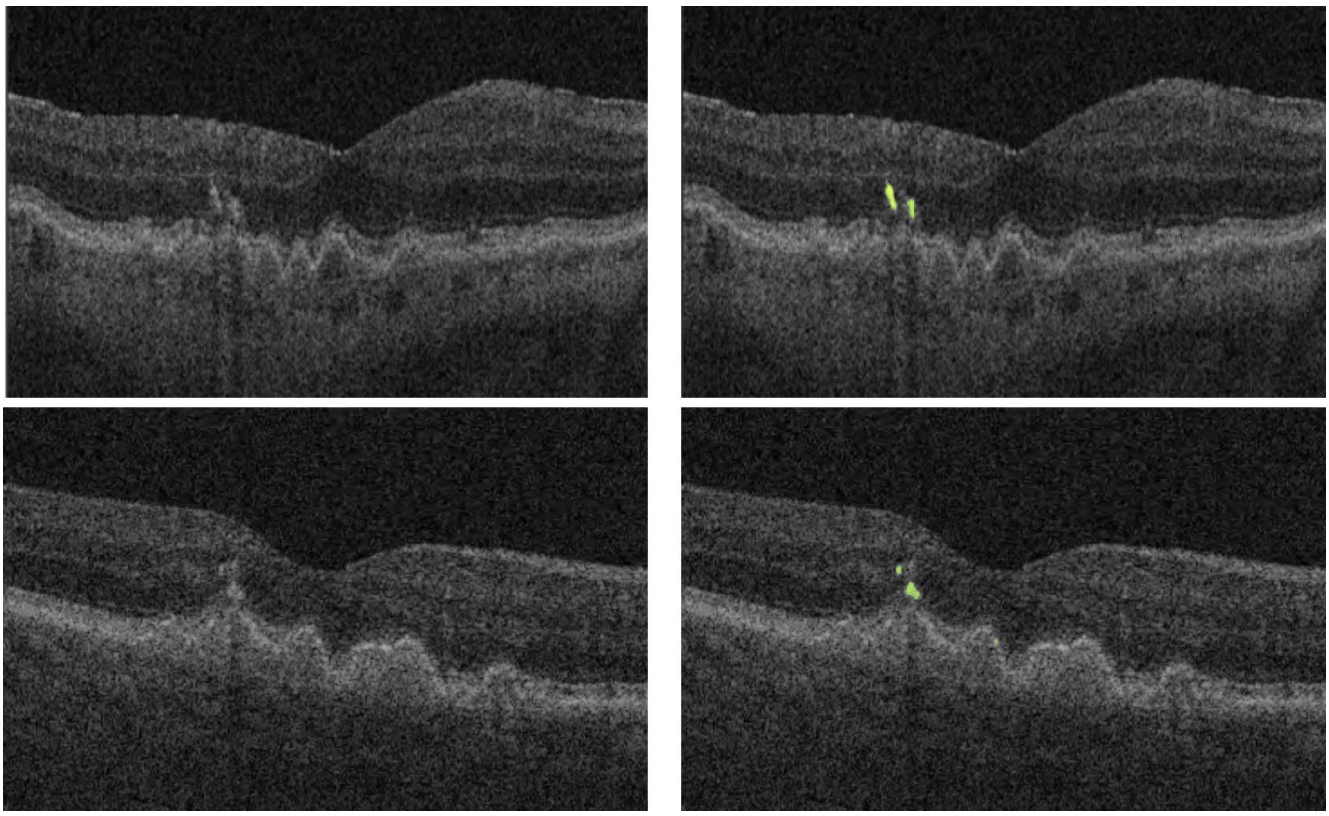

FIGURE 2. Example of automated HRF segmentation (overlaid in *yellow*) within neurosensory layers.

addition, retinal layer and HRF specific features were computed both from retina-wide 2D maps and also from regions limited to just the drusen footprint. An example of a patient with longitudinal 2D feature maps is given in Figure 4. Therefore, for each feature, we measured its mean value and its change in the form of a linear slope during the observation period.

Demographic and Genetic Features. Demographic was information collected from the patients in the HARBOR study, and they were also genotyped. The following three demographic features were used: age, gender, and smoking status. In addition, we used genetic features in the form of a number of risk alleles of single-nucleotide polymorphisms (SNPs) at 34 AMD-associated loci identified in Fritsche et al.[12] A comprehensive list of genetic loci used in our study is shown in Table 2.

Machine Learning. Utilizing the above heterogeneous set of quantitative features, we built a predictive model using machine learning in a supervised setting. Thus, in order to make the predictions, the model first learns the relationship between the time to conversion and a set of features from a training dataset. The model was implemented using a sparse Cox proportional hazards (CPH) model.[13] CPH is the most commonly used multivariable linear model for survival time data; in our case, the eyes were considered to have "survived" until the event of conversion. The CPH model effectively accounts for different individual conversion intervals and the censoring phenomenon, that is, the fact that only some eyes have experienced conversion during the study. The model was regularized with the least absolute shrinkage and selection operator (LASSO), which penalizes the number of features used for the prediction. Such regularization favors simpler

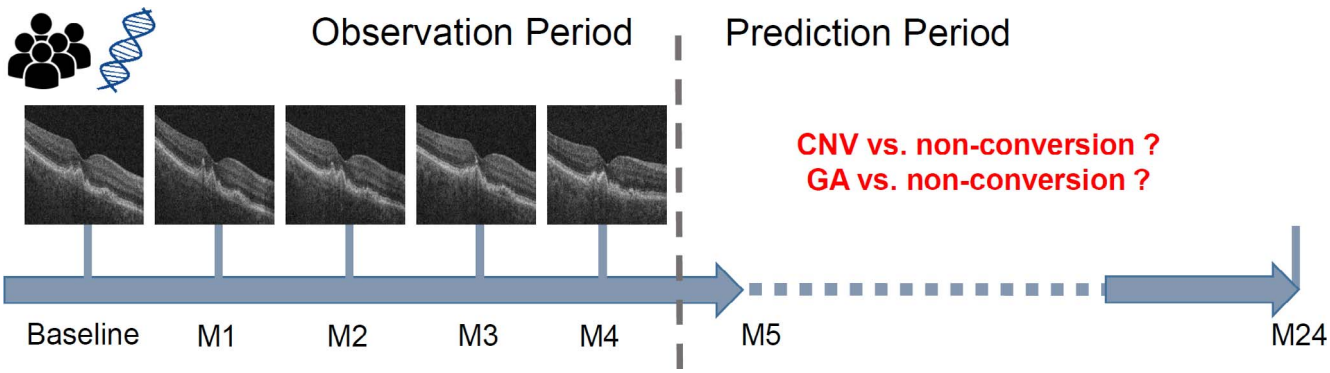

FIGURE 3. Prediction of conversion over 24 months based on heterogeneous feature modeling from baseline through the observation period M1–M4.

Investigative Ophthalmology & Visual Science

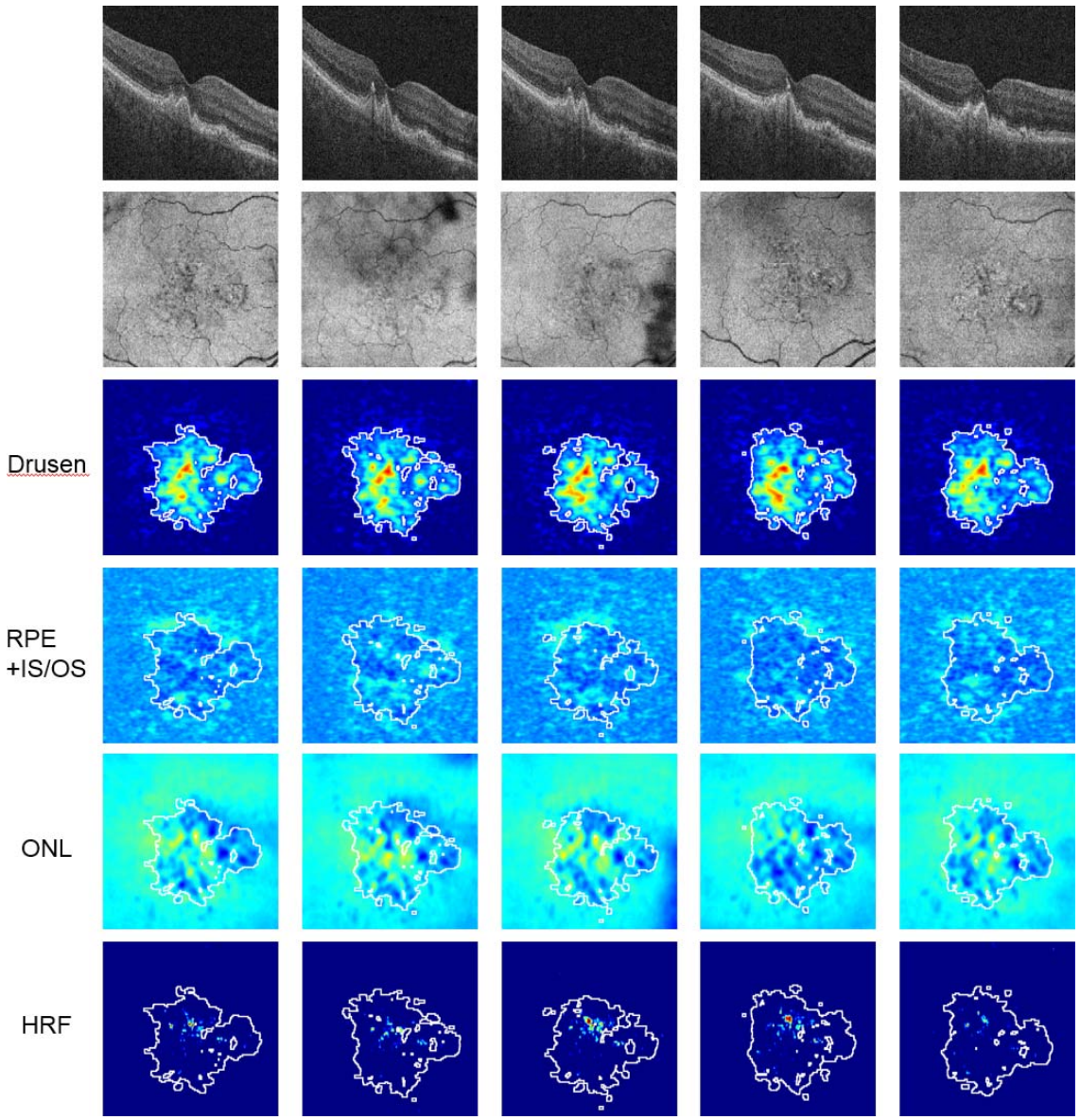

Figure 4. En face 2D thickness maps of relevant imaging biomarkers across the observation period (baseline, month 4) of an individual eye with early AMD. The drusen footprint is delineated in *white*.

models and avoids overfitting the data, at the same time improving the model's interpretability. Once trained, the predictive model produced a hazard ratio (HR) from the input eye features, which we directly used as an index of risk of eye conversion. Two predictive models were independently learned: one for estimating the risk of conversion to CNV, and the other for estimating the risk of conversion to GA.

Statistical Analysis

The performance of the two predictive models was evaluated with a 10-fold cross-validation procedure. In such a procedure, the dataset was randomly partitioned into 10 equal subsets (folds). One fold (10% of eyes) was retained as test set, and the remaining nine folds (90% of eyes) were used for training the model. After 10 iterations, each fold had been tested exactly once, and we obtained a predicted HR index for each eye in the dataset. We performed survival analysis using the predicted HR indices by stratifying the eyes into higher and lower-risk groups and obtaining their survivor functions denoting the probability of nonconversion using Kaplan-Meier estimators. A log-rank test was used to investigate statistical differences in the survival distributions between the two predicted risk groups. In addition, the predicted HR index was used to generate the receiver operating characteristics (ROC) curve to measure the predictive model's classification ability in discriminating the eyes that converted during the trial from the nonconverting eyes. Each point on the ROC curve represents a sensitivity/specificity pair corresponding to a particular decision threshold of the HR index. The classification performance was measured by the area under the ROC curve (AUC), which evaluates the average sensitivity across all false-positive rates. The AUC confidence intervals (CIs) were obtained by bootstrapping with 5000 samples. In addition, specificity at a clinically acceptable sensitivity of 0.80 was reported.[14]

Investigative Ophthalmology & Visual Science

Table 1. Overview of Imaging and Nonimaging Biomarkers and the Number of Quantitative Features Associated

Biomarkers	No.	Feature Description
Imaging		
Drusen	8	Drusen number, total volume and area, maximal height, mean height, height variability (SD), mean, and variability (SD) of internal reflectivity
Pseudodrusen	2	Pseudodrusen number and area
Layer: ONL	5	ONL volume and thicknesses: mean, minimal, maximal, and variability (SD)
Layer: RPE+IS/OS	5	RPE+IS/OS volume and thicknesses: mean, minimal, maximal and variability (SD)
Layer: RPEDC	5	RPE+drusen volume and thicknesses: mean, minimal, maximal, and variability (SD)
HRF	3	HRF in entire retina: total, mean, and variability (SD) of volume and vertical extension
HRF: ONL	3	HRF in ONL: total, mean, and variability (SD) of volume and vertical extension
HRF: RPE+IS/OS	3	HRF in RPE+IS/OS: total, mean and variability (SD) of volume and vertical extension
Nonimaging		
Demographic	3	Age, gender, and smoking status
Genetic	34	SNPs associated with AMD identified in Fritsche et al.[12]

Results

Patient Characteristics

Out of 1095 fellow eyes, 29 were discarded from grading due to a majority of scans missing. After the grading, 452 eyes were excluded as they had bilateral advanced AMD from the onset of the study. A further 39 eyes were discarded as they had already converted during our observation period (month 0 to month 4), and 70 nonconverting eyes were discarded due to absence of drusen. Finally, 10 eyes were eliminated due to poor OCT imaging quality. Thus, data from 495 fellow eyes were used in our study, out of which 159 eyes converted during our prediction period (month 5 to month 24), with 114 primarily converted to CNV and 45 to GA, and 336 eyes with intermediate AMD not having converted by the end of the study. The distribution of conversion incidences throughout the 2-year follow-up is shown in Figure 5. Conversion of intermediate AMD to either CNV or GA occurred throughout the study duration, with the timing uniformly distributed. In this subset of HARBOR fellow eyes, the mean (±SD) age of patients was 78 (±8) years (range, 53–98); 59% were female and 97% were Caucasian. The mean (±SD) baseline visual acuity (VA) was 78 (±10) letters (range, 5–95; Snellen equivalent: 20/30, range, 20/800–20/12).

Table 2. Thirty-Four Genetic Loci Associated With AMD Screened for the Study

Lead Variant	Locus Name
rs429608	SKIV2L
rs4698775	CCDC109B/MCUB
rs10922109	CFH
rs11884770	COL4A3
rs62247658	ADAMTS9-AS2
rs140647181	COL8A1
rs10033900	CFI
rs114092250	PRLR-SPEF2
rs62358361	C9
rs943080	VEGFA
rs7803454	PILRB-PILRA
rs1142	KMT2E-SRPK2
rs79037040	TNFRSF10A
rs71507014	TRPM3
rs10781182	MIR6130-RORB
rs1626340	TGFBR1
rs2740488	ABCA1
rs12357257	ARHGAP21
rs3750846	ARMS2-HTRA1
rs3138141	RDH5-CD63
rs61941274	ACAD10
rs9564692	B3GALTL
rs61985136	RAD51B
rs2043085	LIPC
rs72802342	CTRB2-CTRB1
rs11080055	TMEM97-VTN
rs6565597	NPLOC4-TSPAN10
rs67538026	CNN2
rs2230199	C3
rs429358	APOE
rs142450006	MMP9
rs201459901	C20orf85
rs5754227	SYN3-TIMP3
rs8135665	SLC16A8

Conversion to CNV

Survival functions produced by the predictive model indicating the probability of nonconversion for higher-risk eyes (HR $>$ 1) and lower-risk eyes (HR $<$ 1) are shown in Figure 6a using a Kaplan-Meier plot. The two survival curves indicating the eyes with higher risk and lower risk of CNV conversion were well separated with a statistically significant difference ($P < 0.001$).

The predictive model for conversion to CNV within the prediction period produced an ROC curve with the AUC = 0.68 (CI: 0.62–0.73) as shown in Figure 6b. The operating point that had clinically acceptable sensitivity of 0.80 had a specificity of 0.46.

The importance of features ranked by absolute weight in the predictive model is shown in Figure 6c. Most of the features were positively related with the CNV onset, and furthermore they were mostly focal and obtained from drusen-centric ROI and were not retina-wide. Prediction of CNV was predominantly driven by thickening of the subretinal layers, that is the RPE-drusen complex (RPEDC), an increase in drusen area and an increase in drusen-centric HRF, together with a thickening of the ONL where HRF accumulated. There were no nonimaging features represented among the relevant contributors, indicating that age and genetic features were not contributing to CNV conversion prediction.

Conversion to Geographic Atrophy

Kaplan-Meier plots of survival functions produced by the predictive model indicating the probability of nonconversion to GA for higher-risk eyes (HR $>$ 1), and lower-risk eyes (HR $<$ 1) are shown in Figure 7a. The two survival curves indicating

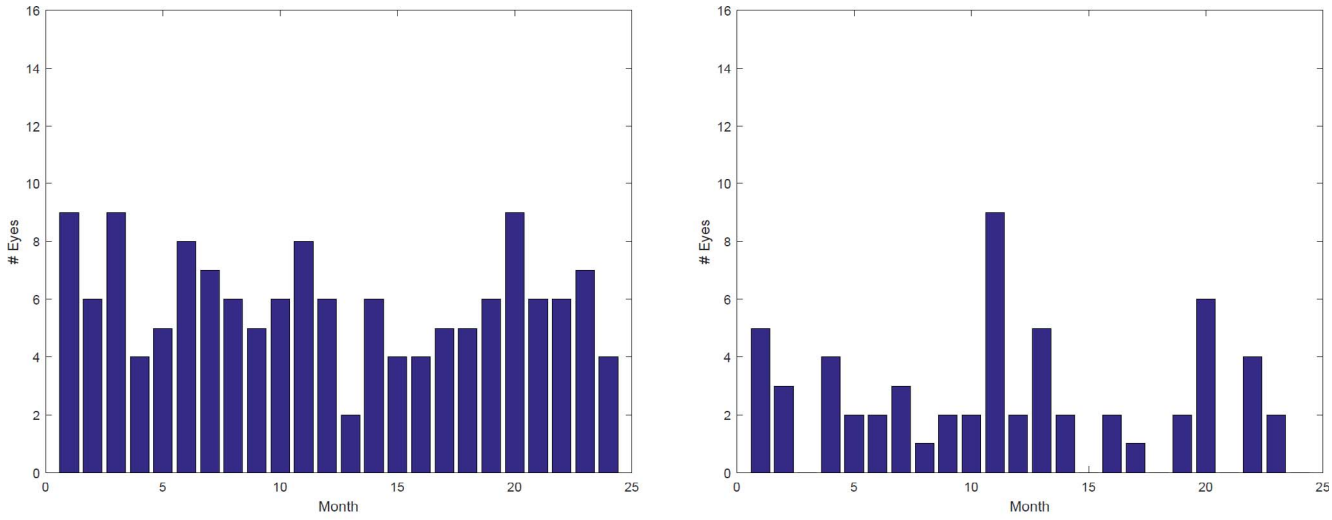

FIGURE 5. Distribution of eyes progressing to late AMD during the study shown for conversion toward CNV (*left*) and GA (*right*).

eyes with higher risk and lower risk of GA conversion were very well and significantly separated ($P < 0.001$).

The predictive model for conversion to GA during the study produced a ROC curve with AUC = 0.80 (CI: 0.73–0.85) as shown in Figure 7b, indicating a high accuracy of risk prediction. The operating point that had clinically acceptable sensitivity of 0.80 had a specificity of 0.69. Thus, the predictive model for GA conversion prediction obtained higher AUC than that for CNV conversion but with wider CIs due to fewer eyes that converted during the study.

Feature importance ranked by absolute weight in the predictive model is shown in Figure 7c. In contrast to the progression profile for CNV, signs of atrophy were among the leading features. Critical features for conversion were outer retinal thinning, including a higher variability in RPE+IS/OS thicknesses and a decrease in the RPE+IS/OS minimal thickness, together with an associated decrease in the thickness of the ONL and an increased presence of HRF at the ONL layer. Furthermore, most features were from retina-wide ROI and not drusen-centric as for CNV. The only relevant nonimaging feature represented was age, and it was an important predictor of GA conversion but not for CNV conversion. Inclusion of genetic features did not benefit the prediction accuracy.

DISCUSSION

In this pioneering work, we were able to introduce a method to determine the individual risk for disease progression in one of the leading causes of visual impairment worldwide, AMD. State-of-the-art means of artificial intelligence were introduced into diagnostic evaluation of retinal morphology, demographics, and genetics. Pathognomonic biomarkers specific for conversion toward CNV or GA were identified and ranked according to their prognostic relevance. This novel tool represents a breakthrough for individual patient counseling and screening, particularly as it can be used on a large scale and is effortless compared to the genetic testing that is currently being suggested to implement personalized medicine in AMD. Establishment of validated machine learning analyses into routine OCT imaging will substantially improve patient care and disease management in AMD with high reliability and expertise.

The HARBOR study offers a unique data set, including a large well-phenotyped and -genotyped population and continuous standardized imaging. From a cohort of 1095 eyes with neovascular AMD and 614 fellow eyes with intermediate AMD, 32% of these fellow eyes converted to late AMD during the 2-year follow-up period: 23.2% to CNV and 9.4% to GA. In the MARINA study, new CNV developed in fellow eyes in 30.9% by 24 months,[15] indicating that the HARBOR conversion scores are in the average range. In general, the risk of neovascular progression is particularly high in fellow eyes of CNV patients, and vision loss in the second eye is then particularly devastating, highlighting the importance of efficient second eye screening in this population providing for earlier intervention and considerably better visual outcomes as shown in the UK Neovascular AMD Database study for a real-world scenario.[16] Following a regular monitoring schedule as in HARBOR, a steady and homogenous rate of conversion for CNV can be expected (Fig. 5), and too-wide intervals for screening should obviously be avoided, questioning the value of quarterly monitoring only. This is particularly true for the distinct group of patients with a high-risk profile.

OCT was shown to offer high sensitivity and specificity for the detection of new-onset CNV in the AMD Detection of Onset of New Choroidal Neovascularization study.[17] Advanced OCT analyses in our study identified a group with a low-risk versus a group with high-risk profile for CNV/GA development. Qualitative and quantitative drusen imaging has been recognized as a key tool in the prognostic evaluation of neovascular AMD progression. Abdelfattah et al.[8] studied the fellow eyes conversion in neovascular AMD and found that eyes with a drusen volume over 0.03 mm^3 had a greater than fourfold higher risk for developing advanced AMD within 24 months using the commercial software of the instrument. In a similarly small CNV cohort, Sisternes et al. used advanced OCT analyses of drusen area, volume, height, and reflectivity to distinguish progressing and nonprogressing cases and achieved an AUC of 0.74 for CNV conversion in 244 eyes.[14] In our much larger population, the AUC for CNV was 0.68, and even higher for the prediction performance of GA with an AUC of 0.80. When we used a similar machine learning algorithm focusing on individual drusen characteristics in 61 eyes, 944 drusen were identified at baseline, out of which 26% regressed, resulting in a predictive AUC of 0.75 within the first 2 years, further highlighting the potential of image-guided prediction of AMD

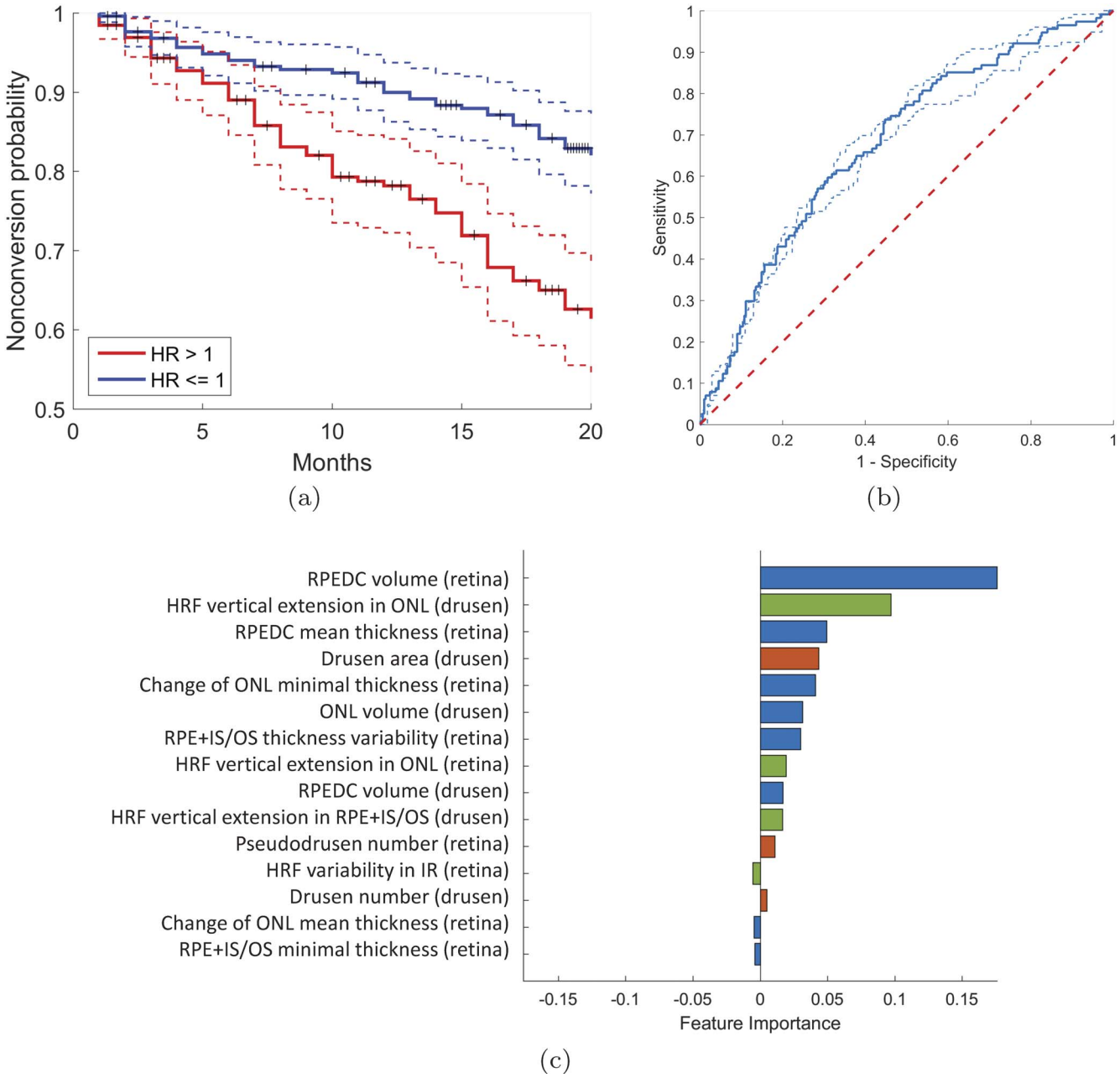

Figure 6. Predictive model of CNV conversion. (**a**) Kaplan-Meier plot with survival curves and their CI (*dotted lines*). (**b**) Receiver operating curve of the predictive model with area under the curve of 0.68 (CI: 0.62–0.73). (**c**) Top 15 most important features with their region of interest drusen-centric or retina-wide, expressed as a mean signed weight assigned to layer-related (*blue*), HRF-related (*green*), and drusen-related (*red*) features.

progression, even on the basis of an individual druse.[18] Our study suggests that an increase in overall drusen load is a key, but not the leading nor the only feature in AMD progression. It is noteworthy that the morphologic changes during the development of CNV were more drusen-centric as drusen area and volume and, particularly, the amount of HRF associated with drusen ranked high, but the alterations seen in GA development were spread retina-wide unrelated to drusen location.

The pathognomonic features associated with AMD progression are manifold and affect neurosensory layers, such as the ONL and the IS/OS line as well as the morphology of the RPE. The extension of neurosensory alteration preexisting before any active disease occurs is impressively visualized in the segmented en face maps produced by image analysis methods (Fig. 4). The primary coexistence of photoreceptor and RPE alteration early on may explain the poor long-term prognosis even with efficient CNV treatment on the long term as well as the simultaneous occurrence of GA despite adequate anti-VEGF therapy,[19] confirmed by our finding of AMD as a disseminated multilayer pathology.

It is interesting that machine learning–based ranking of the morphologic features predicting CNV or GA conversion highlights differential features for the separate pathways that become obvious when comparing the two feature rankings for CNV and GA in Figures 6c and 7c. For CNV conversion, increases in HRF mostly associated with drusen, and to a lesser extent in the overall retina, in number and total volume rank high in predictive value. An increase in volume and mean RPEDC is another prominent feature for CNV development.

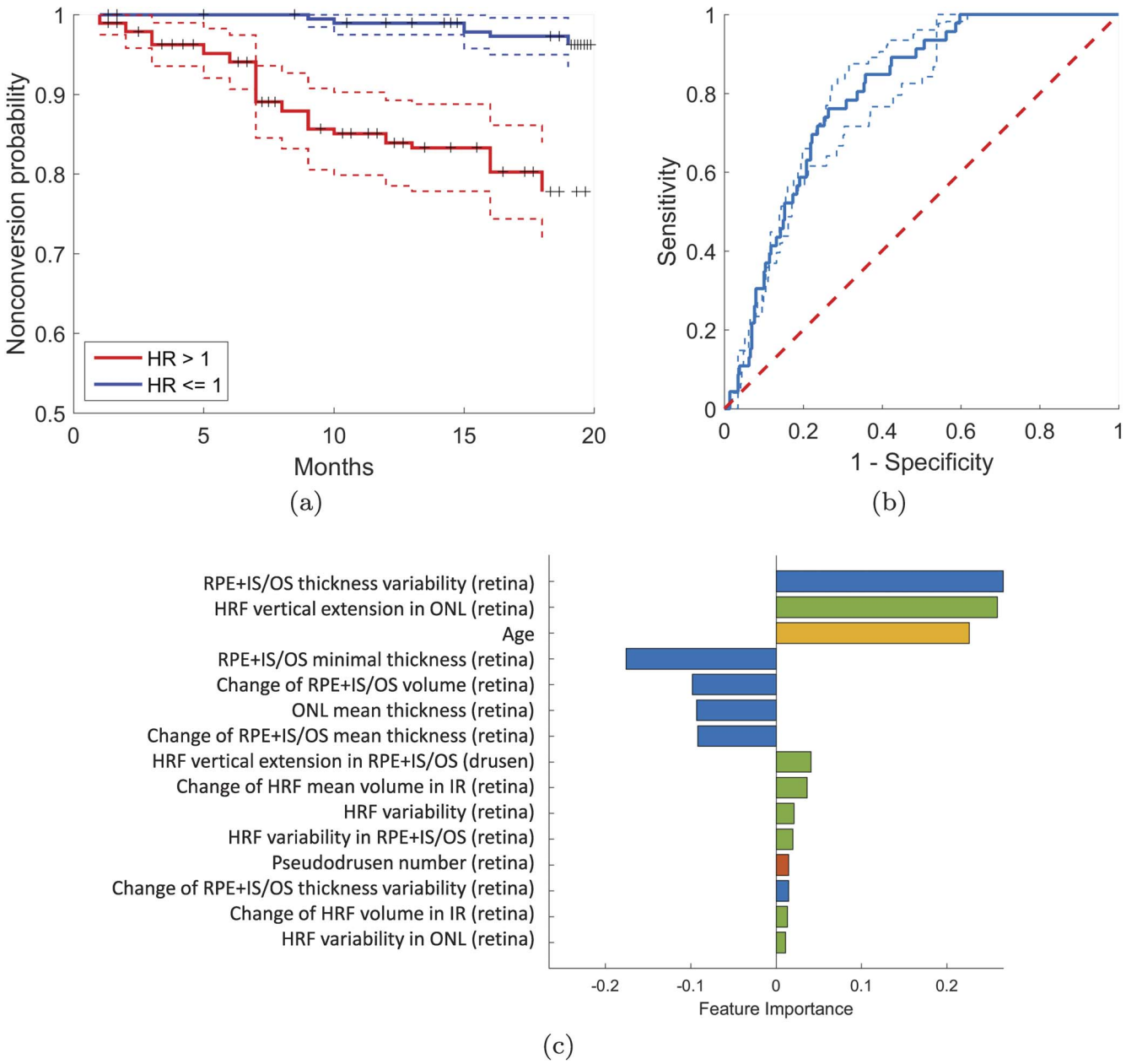

Figure 7. Predictive model of GA conversion. (**a**) Kaplan-Meier plot with survival curves and their CIs (*dotted lines*). (**b**) Receiver operating curve of the predictive model with area under the curve of 0.80 (CI: 0.73–0.85). (**c**) Top 15 most important features with their region of interest drusen-centric or retina-wide, expressed as a mean signed weight assigned to layer-related (*blue*), HRF-related (*green*), drusen-related (*red*), and nonimaging (*yellow*) features.

Drusen area matters substantially, but not the presence of pseudodrusen. An ancillary OCT study on an AREDS population of 265 AMD eyes found a clear association of an increased drusen volume and a 2-year progression to CNV and a quantitative correlation of the risk for CNV development with a 31% increased risk for every 0.1 mm^3-increase in baseline drusen volume.[20] Compared to the ranking of features leading to GA, drusen area/volume, together with overlying HRF, appear to be a distinct pathophysiological hallmark of CNV development. This insight is confirmed by Fragiotta et al.[21] who manually identified HRF as the single most important predicator of neovascular conversion in a retrospective study of 73 eyes over 24 months. Computerized analysis allows corroborating such observations by allowing a comprehensive ranking of all relevant features.

Morphologic conditions predictive for GA development predominantly highlight features of atrophy at the level of the RPE+IS/OS segment, including reduced thickness and volume, irregularity, as well as thinning of the ONL. The fact that age in this context correlates highly with GA development impressively highlights the inevitability of vision loss with advancing age, which is strongly neglected in longevity research. GA is likely a consequence of the general RPE thinning occurring with advancing age as shown in a large cohort of about 70,000 individuals in the UK Biobank study.[22] The ancillary OCT-AREDS study indicated a 32% increase to the odds of developing GA for every 0.001 mm^3 increase in abnormal thinning of the RPE-drusen complex, offering a composite marker of drusen regression with RPE atrophy.[20] The literature regarding risk factors for GA is richer than that for CNV, and the

results are more consistent. Subsidence of the outer plexiform layer and inner nuclear layer was described by Wu et al.[23] as a hallmark of "nascent" GA. A loss in thickness and reflectivity of outer photoreceptor segments and the RPE was identified as the most discriminant early indicator of regions susceptible to GA growth by a study of Niu et al.[24] using fully automated prediction of GA development from quantitative OCT biomarkers. An increase in drusen number does not appear in the ranking of GA-predictive features, yet pseudodrusen, another age-related hallmark, seem to be more relevant for GA progression. HRF are also associated with GA development. Yet, their appearance is rather diffuse throughout all layers of the retina and RPE. HRF were described as precursors of GA development by several authors, such as Christenbury et al.[25] in a study of 299 AMD eyes showing a high correlation of GA development at 2 years with the presence of baseline HRF, greater number of baseline HRF, and greater axial HRF distribution. High-speed ultra-high-resolution OCT depicted HRF as intraretinal RPE migration.[26] A correlation of histology and SD-OCT features by Balaratnasingam et al.[27] confirmed the highly prognostic role of intraretinal RPE cells and suggested HRF monitoring for obtaining a timeline of incipient GA in clinical populations and for anatomic endpoints in clinical trials. The project MACULA by Zanzottera et al.[28] offers a RPE grading system for histology and OCT in AMD explaining the role of RPE shedding and migration as a pathognomonic feature of AMD disease.[28] Advanced imaging analyses easily offer such insight in vivo and over time in an individual patient.

An overwhelming feature in the progression to GA ranking highly in our analyses is the reduction of neurosensory structures. An abnormal thinning of the RPE-photoreceptor interface including the interdigitation of outer segments and RPE apical processes, highly consistent with the segmentation of the RPE+IS/OS layer chosen for our analysis, was described by Sevilla et al.[29] Neurosensory alteration most strikingly reflects early functional loss in GA pathophysiology. Sevilla et al.[29] had already correlated morphologic changes at the RPE-photoreceptor interface with a decrease in cone-mediated sensitivity and rod-mediated dark adaptation time.[29] Tepelus et al.[30] also highlighted the correlation between mesopic retinal sensitivity and OCT metrics of the outer retina in patients with early AMD. Mesopic testing and microperimetry are psychophysical and time-consuming tests; it may be more reliable and feasible to use modern machine learning algorithms for a comprehensive morphologic analysis and pathology staging.

The limitations of this study include the short duration of 2 years and the consequent need to have only a few visits for observation. Obviously, a larger population would be beneficial to reduce the CI width for GA prediction. A further limitation is the performance failure of automated segmentation of discrete features of the retinal layers such as the distinction of HRF close to the RPE and pseudodrusen. However, the consistency of feature detection and their correlation highlight the quality of the data. The AUC in this pioneering work is still limited, but it demonstrates the path to follow and the relevant features and further improvements of the algorithm are ongoing.

In conclusion, we present an innovative approach for predicting the risk of progression from intermediate to advanced AMD that is automated and therefore ideal for large-scale screening in one of the leading diseases of modern times. The population of intermediate AMD individuals included in this study represents the largest cohort analyzed and offers a solid and prospective follow-up obtained by protocol. Machine learning and advanced image analysis based on artificial intelligence allow for a fully automated, fast, and reliable detection of a large spectrum of different features from the neurosensory layer to the RPE, including additional features such as HRF. Most interestingly, differential pathways became visible for the neovascular and the atrophic pathways in AMD: focal decompensation within drusen in CNV as opposed to general retinal ageing in GA. Ageing of the retina is driven by progressive neurodegeneration that can be precisely measured using artificial intelligence tools. In the microcosmos of the eye, computerized image analyses open an entirely new horizon for understanding retinal ageing and disease and offer effective screening and intervention at the earliest time point and at the right therapeutic target.

Acknowledgments

Supported by the Austrian Federal Ministry of Science, Research and Economy.

Disclosure: **U. Schmidt-Erfurth**, Bayer (C), Boehringer Ingelheim (C), Novartis (C); **S.M. Waldstein**, Bayer (C, F), Novartis (C), Genentech (C, F); **S. Klimscha**, None; **A. Sadeghipour**, None; **X. Hu**, None; **B.S. Gerendas**, Roche (C); **A. Osborne**, Genentech (E); **H. Bogunović**, None

References

1. Vos T, Allen C, Arora M, et al. Global, regional, and national incidence, prevalence, and years lived with disability for 310 diseases and injuries, 1990–2015: a systematic analysis for the Global Burden of Disease Study 2015. *Lancet*. 2016;388:1545–1602.
2. Cumberland PM, Rahi JS; for the UK Biobank Eye and Vision Consortium. Visual function, social position, and health and life chances. *JAMA Ophthalmol*. 2016;134:959–966.
3. Ferris FL, Davis MD, Clemons TE, et al. A simplified severity scale for age-related macular degeneration. *Arch Ophthalmol*. 2005;123:1570.
4. Schmidt-Erfurth U, Waldstein SM. A paradigm shift in imaging biomarkers in neovascular age-related macular degeneration. *Prog Retin Eye Res*. 2016;50:1–24.
5. Leuschen JN, Schuman SG, Winter KP, et al. Spectral-domain optical coherence tomography characteristics of intermediate age-related macular degeneration. *Ophthalmology*. 2013;120:140–150.
6. Yehoshua Z, Wang F, Rosenfeld PJ, Penha FM, Feuer WJ, Gregori G. Natural history of drusen morphology in age-related macular degeneration using spectral domain optical coherence tomography. *Ophthalmology*. 2011;118:2434–2441.
7. Nathoo NA, Or C, Young M, et al. Optical coherence tomography-based measurement of drusen load predicts development of advanced age-related macular degeneration. *Am J Ophthalmol*. 2014;158:757–761.e1.
8. Abdelfattah NS, Zhang H, Boyer DS, et al. Drusen volume as a predictor of disease progression in patients with late age-related macular degeneration in the fellow eye. *Invest Ophthalmol Vis Sci*. 2016;57:1839–1846.
9. De Fauw J, Keane P, Tomasev N, et al. Automated analysis of retinal imaging using machine learning techniques for computer vision. *F1000Research*. 2016;5:1573.
10. Li K, Wu X, Chen DZ, Sonka M. Optimal surface segmentation in volumetric images–a graph-theoretic approach. *IEEE Trans Pattern Anal Mach Intell*. 2006;28:119–134.
11. Schlegl T, Waldstein SM, Bogunovic H, et al. Fully automated detection and quantification of macular fluid in OCT using deep learning. *Ophthalmology*. 2018;125:549–558.
12. Fritsche LG, Igl W, Bailey JNC, et al. A large genome-wide association study of age-related macular degeneration highlights contributions of rare and common variants. *Nat Genet*. 2016;48:134–143.

13. Hastie T, Tibshirani R, Wainwright M. *Statistical Learning with Sparsity: The Lasso and Generalizations*. Boca Raton, FL: CRC Press; 2015.
14. de Sisternes L, Simon N, Tibshirani R, Leng T, Rubin DL. Quantitative SD-OCT imaging biomarkers as indicators of age-related macular degeneration progression. *Invest Ophthalmol Vis Sci*. 2014;55:7093–7103.
15. Barbazetto IA, Saroj N, Shapiro H, Wong P, Ho AC, Freund KB. Incidence of new choroidal neovascularization in fellow eyes of patients treated in the MARINA and ANCHOR trials. *Am J Ophthalmol*. 2010;149:939–946.e1.
16. Zarranz-Ventura J, Liew G, Johnston RL, et al. The neovascular age-related macular degeneration database: report 2: incidence, management, and visual outcomes of second treated eyes. *Ophthalmology*. 2014;121:1966–1975.
17. Do DV, Gower EW, Cassard SD, et al. Detection of new-onset choroidal neovascularization using optical coherence tomography. *Ophthalmology*. 2012;119:771–778.
18. Bogunovic H, Montuoro A, Baratsits M, et al. Machine learning of the progression of intermediate age-related macular degeneration based on OCT imaging. *Invest Opthalmol Vis Sci*. 2017;58:BIO141–BIO150.
19. Rofagha S, Bhisitkul RB, Boyer DS, Sadda SR, Zhang K; SEVEN-UP Study Group. Seven-year outcomes in ranibizumab-treated patients in ANCHOR, MARINA, and HORIZON. *Ophthalmology*. 2013;120:2292–2299.
20. Folgar FA, Yuan EL, Sevilla MB, et al. Drusen volume and retinal pigment epithelium abnormal thinning volume predict 2-year progression of age-related macular degeneration. *Ophthalmology*. 2016;123:39–50.e1.
21. Fragiotta S, Rossi T, Cutini A, Grenga PL, Vingolo EM. Predictive factors for development of neovascular age-related macular degeneration: a spectral-domain optical coherence tomography study. *Retina*. 2017:38:245–252.
22. Ko F, Foster PJ, Strouthidis NG, et al. Associations with retinal pigment epithelium thickness measures in a large cohort: results from the UK Biobank. *Ophthalmology*. 2017;124:105–117.
23. Wu Z, Luu CD, Ayton LN, et al. Optical coherence tomography-defined changes preceding the development of drusen-associated atrophy in age-related macular degeneration. *Ophthalmology*. 2014;121:2415–2422.
24. Niu S, de Sisternes L, Chen Q, Rubin DL, Leng T. Fully automated prediction of geographic atrophy growth using quantitative spectral-domain optical coherence tomography biomarkers. *Ophthalmology*. 2016;123:1737–1750.
25. Christenbury JG, Folgar FA, O'Connell RV, Chiu SJ, Farsiu S, Toth CA. Progression of intermediate age-related macular degeneration with proliferation and inner retinal migration of hyperreflective foci. *Ophthalmology*. 2013;120:1038–1045.
26. Ho J, Witkin AJ, Liu J, et al. Documentation of intraretinal retinal pigment epithelium migration via high-speed ultra-high-resolution optical coherence tomography. *Ophthalmology*. 2011;118:687–693.
27. Balaratnasingam C, Messinger JD, Sloan KR, Yannuzzi LA, Freund KB, Curcio CA. Histologic and optical coherence tomographic correlates in drusenoid pigment epithelium detachment in age-related macular degeneration. *Ophthalmology*. 2017;124:644–656.
28. Zanzottera EC, Messinger JD, Ach T, Smith RT, Freund KB, Curcio CA. The project MACULA retinal pigment epithelium grading system for histology and optical coherence tomography in age-related macular degeneration. *Invest Ophthalmol Vis Sci*. 2015;56:3253–3268.
29. Sevilla MB, McGwin G, Lad EM, et al. Relating retinal morphology and function in aging and early to intermediate age-related macular degeneration subjects. *Am J Ophthalmol*. 2016;165:65–77.
30. Tepelus TC, Hariri AH, Al-Sheikh M, Sadda SR. Correlation between mesopic retinal sensitivity and optical coherence tomographic metrics of the outer retina in patients with non-atrophic dry age-related macular degeneration. *Ophthalmic Surg Lasers Imaging Retina*. 2017;48:312–318.

Investigative Ophthalmology & Visual Science